THE JOURNAL OF PHYSICAL CHEMISTRY A

Article

Cite This: J. Phys. Chem. A 2019, 123, 1710−1719

pubs.acs.org/JPCA

Two-State, Three-Mode Parametrization of the Force Field of a Retinal Chromophore Model

Emanuele Marsili,[†] Marwa H. Farag,[¶] Xuchun Yang,[‡] Luca De Vico,[†] and Massimo Olivucci*[,†,‡,§]

[†]Dipartimento di Biotecnologie, Chimica e Farmacia, Università di Siena, via A. Moro 2, I-53100 Siena, Italy

[¶]Department of Chemistry, University of Southern California, Los Angeles, California 90089-0482, United States,

[‡]Department of Chemistry, Bowling Green State University, Bowling Green, Ohio 43403, United States and

[§]Institut de Physique et Chimie des Matériaux de Strasbourg, UMR 7504, Université de Strasbourg-CNRS, F-67034 Strasbourg, France

Supporting Information

ABSTRACT: In recent years, the potential energy surfaces of the penta-2,4-dieniminium cation have been investigated using several electronic structure methods. The resulting pool of geometrical, electronic, and energy data provides a suitable basis for the construction of a topographically correct analytical model of the molecule force field and, therefore, for a better understanding of this class of molecules, which includes the chromophore of visual pigments. In the present contribution, we report the construction of such a model for regions of the force field that drive the photochemical and thermal isomerization of the central double bound of the cation. While previous models included only two modes, it is here shown that the proposed three-mode model and corresponding set of parameters are able to reproduce the complex topographical and electronic structure features seen in electronically correlated data obtained at the XMCQDPT2//CASSCF/6-31G* level of theory.

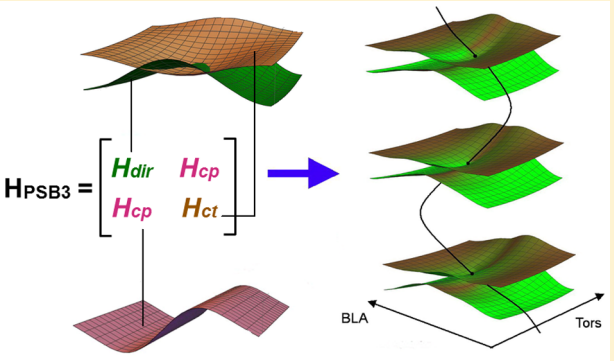

1. INTRODUCTION

The penta-2,4-dieniminium cation (PSB3) is a minimal homologue[1−6] of the chromophore of visual pigments: the 11-*cis* protonated retinal Schiff base (PSB11). Indeed, 2-*cis*-PSB3 (see Scheme 1) reproduces several features of more realistic PSB11 models such as the 4-*cis*-nona-2,4,6,8-tetraeniminium cation, which incorporates five of the six PSB11 double bonds.[7−10] Furthermore, PSB3 features two barrier-less singlet excited state (S_1) paths that drive the 2-*cis* to all-*trans* and the all-*trans* to 2-*cis* photochemical isomerizations, respectively and thus mimics the biologically important PSB11 and PSBAT (i.e., the all-*trans* protonated retinal Schiff base) photoisomerizations.

Scheme 1. Photochemical and Thermal Double-Bond Isomerizations of PSB3

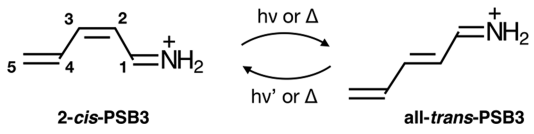

Recent systematic studies[11,12] have shed light on the topography of the ground state (S_0) and the lowest singlet excited state (S_1) potential energy surfaces (PESs) of PSB3. More specifically, the regions describing the isomerization of the central C2═C3 double-bond of PSB3 (see Scheme 1) have been mapped at the CASSCF level and, partially, at the CASPT2 level along six paths.[12] The corresponding energy profiles have then been computed using a variety of electronic structure methods[11−16] to assess their ability to reproduce the energy profiles computed at the MRCISD+Q[17,18] level of theory, which is assumed to be accurate.

As shown in Figure 1, the six paths include two intrinsic reaction coordinates (MEPcis and MEPtrans) describing the cis → trans and trans → cis isomerization on the S_1 PES, two intrinsic reaction coordinates (MEPct and MEPdir) documenting the cis → trans and trans → cis isomerizations on the S_0 PES and two interpolated paths (IS and BLAP) connecting the S_1 and S_0 pairs of intrinsic reaction coordinates of PSB3. These interpolated paths are chemically significant: the first path (IS) is part of the PSB3 S_1/S_0 intersection space (a 3N-8 dimensional space formed by conical intersection points with N being the number of nuclei) that drives the photochemical isomerization. The second path (BLAP) connects the covalent/diradical (TSdir) and charge-transfer (TSct) S_0 transition states that controls the thermal isomerization, and

Received: October 14, 2018
Revised: January 18, 2019
Published: February 12, 2019

DOI: 10.1021/acs.jpca.8b10010
J. Phys. Chem. A 2019, 123, 1710−1719

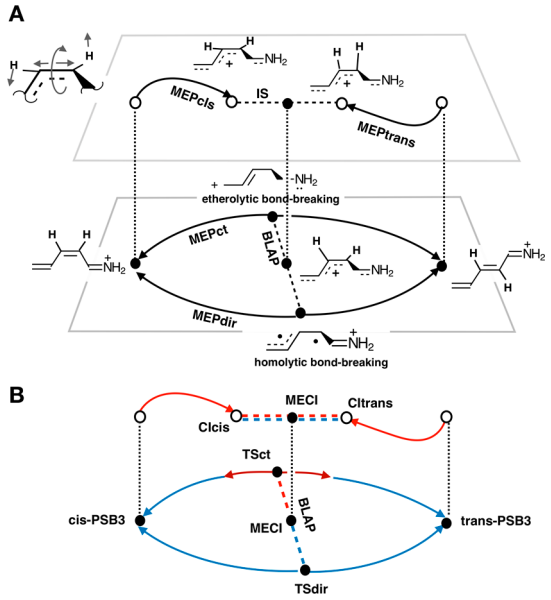

Figure 1. Schematic illustration of the relationship between the six interconnected PSB3 paths considered in the present work. (A) Geometrical changes. Full circles indicate the stationary points located along the S_1 (upper deck) or S_0 (lower deck) PESs or along the S_1/S_0 intersection space where, by definition the S_1 and S_0 energies are identical. Open circles indicate nonequilibrium structures. Dashed lines represent interpolated paths. The vertical dotted lines indicate points with identical geometry. The top-left structure represents the dominating geometrical changes of the reacting fragment. (B) Electronic structure changes along the same paths. Blue lines represent paths dominated by a COV/DIR character. Red lines mark paths or path segments dominated by a CT character. The double red/blue dashed segment represents the S_1 and S_0 energy degeneracy along the intersection space, which have mixed CT and COV/DIR characters. CIcis and CItrans are the conical intersections located at the end of MEPcis and MEPtrans paths and mediate the 2-*cis* to all-*trans* and all-*trans* to 2-*cis* photoisomerizations, respectively.

passes through the geometry of the minimum energy conical intersection[19] (MECI), i.e., the local minimum of the aforementioned intersection space.

The major geometrical changes along the different paths[12] are schematically illustrated in Figure 1A. These are characterized by (i) a stretching motion corresponding to a change in bond length alternation along the PSB3 backbone (BLA), (ii) an out-of-phase wag of the hydrogen atoms bounded to the reactive C2 = C3 bond (HOOP) and (iii) the torsion about C2═C3 (Torsion). Such geometrical changes are accompanied by variations in the electronic character along the S_1 and S_0 PESs (see Figure 1B). For instance, along the MEPcis and MEPtrans paths there is a change in the charge-transfer (CT) character with respect to the S_0 equilibrium structures. This is apparent in Figure 1A by comparing the upper deck CT resonance structures with the corresponding lower deck 2-*cis* reactant and all-*trans* product resonance structures. Conversely, MEPdir, which incorporates TSdir, features a covalent/diradical (COV/DIR) character, where the π-electrons are distributed as in the S_0 equilibrium structures. Finally, and most remarkably, MEPct, which incorporates TSct, features the same CT character of the S_1 paths in the transition state region, but switches to a COV/DIR character in the vicinity of 2-*cis*-PSB3 or all-*trans*-PSB3. As indicated in Figure 1A, these results are consistent with TSdir and TSct mediating a homolytic and heterolytic bond breaking, respectively.

The above revised results suggest that the photochemical and thermal reactivity of PSB3 can be captured by a model force field based on three modes (i.e., geometrical coordinates) and two electronic states with varying electronic characters. The availability of an analytical expression for such simplified model force field, would permit to carry out, otherwise time-costly studies of time-dependent dynamical processes of PSB11 and PSBAT.

Below we show that the above-described paths give access to the parametrization of an analytical model of the S_1 and S_0 PESs of PSB3. While not aiming to a quantitative model, we here pursue a model that can be realistically used for the systematic investigation of the effects of the PESs three-dimensional topography on the isomerization mechanism/dynamics of the central C2═C3 bond. The model must thus provide a qualitatively correct representation of the energy, geometry, and electronic structure changes occurring during the photochemical and thermal double-bond isomerizations.

The parametrization of our two-state three-mode models is based on the pool of points provided by the six paths introduced above. In the following, such pool of data will be called *data set*. The consequently obtained force field model should make possible to reproduce the data set's topographic (e.g., excitation energies and barrier) and electronic (e.g., charge distribution) features. This should remove some limitations of the two-state two-mode model originally proposed by Stock and co-workers[20] that, due to its mathematical convenience, has nevertheless been used in several quantum dynamics studies of the retinal chromophore.[21−25] In fact, as later discussed, the Stock model only accounts for a torsional (isomerization) mode and a stretching mode. Finally, we note that analytical two-state three-mode models of the retinal chromophore have been previously proposed.[26,27] However, such models were not based on extensive quantum chemical calculations but incorporated experimentally determined parameters.

2. METHODS

Our parametrization is defined by (i) the electronic structure method employed to compute the necessary S_0 and S_1 adiabatic energies, (ii) the expression of the three independent geometrical variables (BLA, HOOP, and Torsion), (iii) the expression of a factor representing the character of the adiabatic electronic state at each point and (iv) the definition of diabatic states. Points i−iii are discussed in subsection 2.1, while point iv is discussed in subsection 2.2. Finally, in subsection 2.3, we give the expression of the diabatic states and the coupling between them, in term of geometrical coordinates.

Before presenting the technical subsections listed above, we quickly review the Stock model. Such model is defined by a Hamiltonian, where the diagonal elements represent the energies of diabatic states and the off-diagonal elements represent their electronic coupling.[19] The diagonal elements are expressed as the sum of simple cosine functions depending on the isomerization mode and a quadratic term depending on the stretching mode. One of the two diagonal elements also contains a third term corresponding to a linear function of the stretching mode. In total, the diagonal elements contain five different fitting parameters. The identical off-diagonal elements are, instead, expressed in terms of a linear function of the

DOI: 10.1021/acs.jpca.8b10010
J. Phys. Chem. A 2019, 123, 1710−1719

stretching mode and contain just one fitting parameter. Notice that in the Stock model, the S_0 reactant and product lie in different diabatic states that cross along the torsional mode. Because of this property, such states cannot be associated with the CT and COV/DIR electronic structures discussed above (i.e., by definition the reactant and product have the same COV/DIR electronic structure). In contrast, in our model we associate the diabatic states to electronic configurations featuring different charge distributions. Such states represent the starting points for the discussion of the electrostatic effects imposed by the protein cavity on the retinal chromophore: a basic point when discussing the impact of mutations leading to red- or blue-shifted absorbance.

2.1. Geometrical Variables and Electronic Character. Among the various electronic structure methods employed to compute the PSB3 S_1 and S_0 PESs (we assume that S_2 and higher states have no effect on the isomerization dynamics as reported for visual pigments; see also the final paragraph of section 4 and the Supporting Information),[12] XMCQDPT2[28] energy profiles showed a close agreement with MRCISD+Q, considered as the most accurate method. Also, in contrast with other methods providing electron correlation corrections such as CASPT2 and MRCISD+Q, it yields a correct conical intersection topology.[28,29] Thus, the primary target of this work is to construct a model Hamiltonian (H_{PSB3}) capable of simulating the XMCQDPT2 energy trends provided by the data set (e.g., the adiabatic energy profiles along the six paths introduced above). When necessary (see below) new XMCQDPT2 calculations have been carried out with the quantum chemical package Firefly,[30] which is partially based on the Gamess US source code.[31]

The analysis of the geometrical changes along the six paths discussed in the introduction, points to three leading geometrical variables: the BLA, HOOP, and Torsion already mentioned above. As shown by the definitions given in Figure 2A, the values of these variables can be obtained from the internal coordinates of the data set.

As we will detail below, the matrix elements of H_{PSB3} are functions of BLA, HOOP and Torsion which, starting with subsection 2.2, have been renamed, for simplicity, r, φ, and θ respectively. In Figure 2B, we indicate the leading variables characterizing the changes along each path.[11,12] For instance, MEPcis and MEPtrans are initially led by BLA, which decreases in value due to a double-bond/single-bond inversion motion. After such process, a combination of HOOP, and Torsion dominates until CIcis and CItrans (see Figure 1) are reached. These conical intersections are connected through combined HOOP and Torsion changes along IS, while BLA remains substantially constant. The BLAP path connecting TSdir and TSct on the S_0 PES has the opposite behavior. In this case, HOOP and Torsion remain constant at 0° and −90°, respectively, while the geometrical change is mainly characterized by a BLA variation.

In Figure 2B, we also provide a schematic representation of the change in electronic character[12] (or diabatic state) along the paths. The weight of a diabatic state is determined by computing the fraction of positive charge residing on the PSB3 moiety containing the nitrogen atom (C2H−C1H−NH_2 in Scheme 1). Along the IS and at TSdir and TSct (i.e., for all structures with Tors featuring a 90° value) such moiety is either charged +1 (corresponding to a pure COV/DIR character) or 0 (indicating a full CT character). In valence-bond terms, such charges correspond to resonance structures

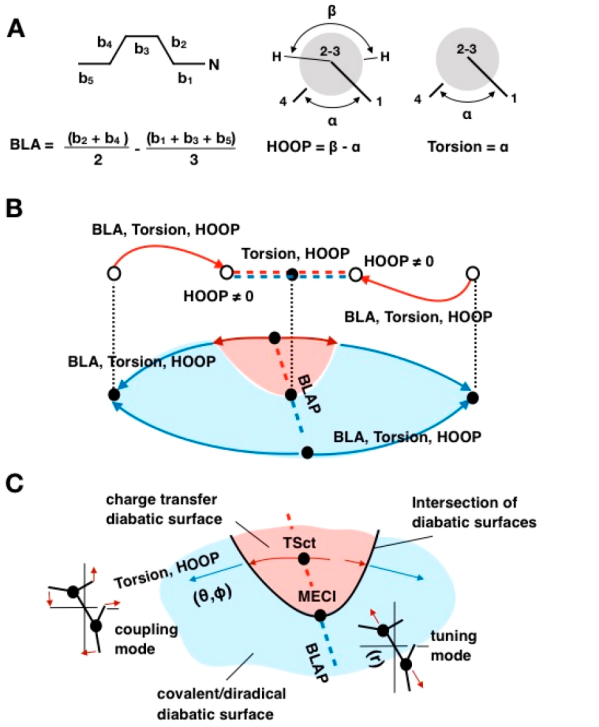

Figure 2. Geometrical variables and diabatic states. (A) Geometrical coordinates used in the parametrization of the model Hamiltonian. (B) Coordinates contributing to each path in the data set (see legend of Figure 1 for the symbols). The relationship between paths and $\Psi_{COV/DIR}$ and Ψ_{CT} diabatic states (electronic characters) is illustrated for the S_0 PES. The red regions are dominated by Ψ_{CT} while the blue regions are dominated by $\Psi_{COV/DIR}$. (C) Details of the Ψ_{CT} dominated region of the S_0 PES. At MECI, a pseudo totally symmetric tuning mode is associated with BLA while the coupling mode is associated with a nontotally symmetric mode featuring HOOP and Torsion contributions. In the following BLA, HOOP, and Torsion are renamed r, φ, and θ respectively.

describing TSdir (homolytic bond breaking) and TSct (heterolytic bond breaking) in Figure 1A.

Along MEPcis and MEPtrans as well as MEPdir and MEPct, the value of the charge of C2H−C1H−NH_2 changes. For instance, when starting from TSct and following MEPct path, its value goes from a dominating CT character (red region) to a dominating COV/DIR character (blue region). The S_0 CT region has a vertex at MECI and expands toward TSct delimiting a charge-transfer region (see Figure 2B). In contrast, when moving along MEPdir the COV/DIR character remains dominating.

Notice that previous results on QM/MM models of the full visual pigment and/or full chromophore showed that the PES topography described above is general for polyeniminium cations (N-protonated or *N*-alkylated polyene Schiff bases) and it is not limited to PSB3.

2.2. Structure of the Model Hamiltonian. The proposed parametrization is based on a two-state electronic Hamiltonian H_{PSB3} whose diagonal matrix elements *Hdir* and *Hct* correspond to the energies of the diabatic electronic states,[32] while the off-diagonal matrix element *Hcp* represents their coupling. As anticipated above we write these matrix elements as functions of $r \equiv$ BLA, $\varphi \equiv$ HOOP, and $\theta \equiv$ Torsion (see Figure 2A) which contain parameters whose values are determined via a fitting protocol. It follows that the eigenvalues of the corresponding secular equation provide the simulated S_0

DOI: 10.1021/acs.jpca.8b10010
J. Phys. Chem. A 2019, 123, 1710−1719

and S_1 adiabatic PESs, while the eigenvectors provide information on the corresponding electronic characters.

As anticipated above, a key point in the construction of H_{PSB3} is the definition of the diabatic electronic states. Since diabatic states are only a mathematical construct, they can be formulated without a specific meaning. Instead, we adopt a property-based definition[32] based on the magnitude of the total charge residing on the C2H−C1H−NH_2 moiety of PSB3. More specifically, the diabatic states $\Psi_{COV/DIR}$ and Ψ_{CT} are associated with a fragment (i.e., C2H−C1H−NH_2) charge equal to 0 and +1, respectively. Accordingly, the regions of the adiabatic PESs featuring a mixed electronic character (0 < charge < + 1) must be described by linear combinations of $\Psi_{COV/DIR}$ and Ψ_{CT} with weights provided by the eigenvectors of the model Hamiltonian. Josef Michl and Vlasta Bonačić-Koutecký have originally described the electronic states driving the photoisomerization of model retinal chromophores.[33]

In order to propose an expression for *Hdir* and *Hct*, i.e., for the diabatic PESs associated with $\Psi_{COV/DIR}$ and Ψ_{CT}, we have chosen *r* as the (pseudo) totally symmetric *tuning* mode[34,35] (see BLAP direction in Figure 2C). This appears to be a convenient choice as the charge distribution extracted from the data set shows that along BLAP the adiabatic states are substantially pure diabatic states. Furthermore, when starting from TSdir on the S_0 PES and move toward TSct, the electronic character switches from pure $\Psi_{COV/DIR}$ to pure Ψ_{CT} at MECI. Accordingly, the off-diagonal matrix element *Hcp* must be zero along BLAP and whenever the value of φ and θ are simultaneously 0° and 90°, respectively.

As illustrated in Figure 2C, the two diabatic PESs must cross in a direction orthogonal to BLAP forming an intersection. In the vicinity of MECI, such direction corresponds to a combination of φ and θ defined as the *coupling* mode (i.e., in a direction orthogonal to BLAP in Figure 2C).[34,35] The computed adiabatic energies show that when moving along such mode the S_1 and S_0 adiabatic energies split. *Hcp* must therefore increase from zero to nonzero values along such mode.

In order to account for the above data set features during the parametrization, we impose the following constraints on the expressions of *Hdir*, *Hct* and *Hcp*: (i) $Hcp = 0$ when $\varphi = 0°$ and $\theta = \pm 90°$ (i.e., along the tuning mode), (ii) *Hcp* increases when moving along the coupling mode, and (iii) *Hcp* is independent from *r*. As we will discuss below, we also impose an extra constraint which is not fully consistent with the information found in the data set: (iv) at the S_0 equilibrium structures of 2-*cis*-PSB3 and all-*trans*-PSB3, the S_0 and S_1 states correspond to pure $\Psi_{COV/DIR}$ and Ψ_{CT} diabatic states, respectively.

As illustrated in Figure 2C, the diabatic PESs cross along a line spanning a range of θ and φ values. This is reasonable when considering that one follows the diabatic states over a large region of the configuration space on both the S_1 and S_0 PESs. We stress that the diabatic crossing produced by the proposed Hamiltonian is ultimately determined by the fitting protocol and is not imposed by the model.

2.3. Expressions of the Diabatic functions and Coupling Term. As previously mentioned, the diagonal matrix elements *Hdir* and *Hct* are functions of *r*, θ, and φ. However, since the data set indicates that *r* and φ are weakly coupled, the expression of *Hdir* and *Hct* have been written as

$$H_{PSB3} = \begin{bmatrix} Hdir & Hcp \\ Hcp & Hct \end{bmatrix} \quad (1)$$

$$Hct = Hct2D + Hct_{corr} \quad (2)$$

$$Hdir = Hdir2D + Hdir_{corr} \quad (3)$$

Here, *Hdir*2D and *Hct*2D are functions of *r* and θ exclusively. Since the φ coordinate contributes to determine the π-overlap across the reactive double bond, it must affect the diabatic energies when its value is different from zero (i.e., when the π-orbitals interacting across the reactive double bound are orthogonal). Accordingly, the dependence of *Hdir* and *Hct* on φ is introduced via the terms $Hdir_{corr}$ and Hct_{corr}. *Hdir*2D and *Hct*2D can be then seen as the analogue of the diagonal elements of the Stock's model, while the correction functions are employed to account for the φ dependence seen in the data set.

The four terms *Hdir*2D, *Hct*2D, $Hdir_{corr}$, and Hct_{corr} were defined using the following functional forms:

$$Hdir2D(r, \theta) = \sin\left[\frac{\pi\theta}{180}\right]^2 (d_1 r^2 + d_2) + d_3 \cos\left[\frac{\pi\theta}{360}\right] + d_4 (r - 0.091)^2 \quad (4)$$

$$Hct2D(r, \theta) = \left(1 + c_5 \sin\left[\frac{\pi\theta}{180}\right]^2\right)(c_1 r^2 + c_2 r + c_3) + c_4 \cos\left[\frac{\pi\theta}{180}\right] \quad (5)$$

$$Hdircorr(\phi, \theta) = hd_1 \sin\left[\frac{\pi\phi}{360}\right]^2 - hd_2 \sin\left[\frac{\pi\phi}{360}\right] \sin\left[\frac{\pi\theta}{90}\right] \quad (6)$$

$$Hctcorr(\phi, \theta) = hc_1 \sin\left[\frac{\pi\phi}{360}\right]^2 + hc_2 \sin\left[\frac{\pi\phi}{360}\right] \sin\left[\frac{\pi\theta}{90}\right] \quad (7)$$

Finally, the expression of the electronic coupling is

$$Hcp(\phi, \theta) = \left(1 + k_2 \sin\left[\frac{\pi\theta}{180}\right]^2\right) k_1 \sin\left[\frac{\pi(-\phi/2 + \theta)}{90}\right] \quad (8)$$

These expressions contain a total of 15 parameters (*c*, *d*, *hc*, *hd*, and *k* parameters) whose values are found by fitting the data set (see next subsection). The significance of the most relevant parameters will be discussed in section 3.

2.4. Fitting Protocol. Each data set point contains one set of nuclear coordinates, the associated S_0 and S_1 adiabatic energies and the corresponding atomic charges. All quantities were computed at the XMCQDPT2//CASSCF/6-31G* level (i.e., the nuclear coordinates were computed at the CASSCF level and the energies through single point XMCQDPT2 calculations). The reason for using the modest 6-31G* basis set has been explained in ref 11 (see Table 2 in ref 11) and it is justified by the fact that, mainly due to a cancellation of errors, the 6-31G* basis set is rather accurate (with respect to MR-CISD+Q energies) in regions not too far from the FC point and provide a qualitatively correct description also in regions that are far from it.

DOI: 10.1021/acs.jpca.8b10010
J. Phys. Chem. A 2019, 123, 1710−1719

For each point, the corresponding values of r, θ, and φ were determined using the definitions in Figure 2A. Similarly, the electronic character of the S_0 and S_1 adiabatic states were determined by calculating the total Mulliken atomic charge of the C2H−C1H−NH_2 moiety. The fitting of the entire data set required four steps:

I Selection from the data set of a subset of "diabatic points" where the adiabatic states are assumed to correspond to the $\Psi_{COV/DIR}$ or Ψ_{CT} states. The set comprises the first 11 points of MEPcis and MEPtrans and all 14 BLAP points for a total of 36 points. All diabatic points have $\varphi = 0°$. Moreover, the MEPcis, BLAP, and MEPtrans diabatic points have approximately $\theta = 0°$, $\theta = -90°$, and $\theta = -180°$, respectively.

II Parametrization of *Hct*2D and *Hdir*2D. *Hct*2D and *Hdir*2D feature a total of nine parameters (c_1−c_5 and d_1−d_4) whose values are determined by fitting the 36 "diabatic points" defined in I.

III Expression of *Hdir* and *Hct*. The parametrized functions, *Hdir*2D and *Hct*2D, are then added to $Hdir_{corr}$ and Hct_{corr} respectively, to obtain the final expression of the diagonal matrix elements of H_{PSB3}. These two expressions contain other four parameters hc_1−hc_2 and hd_1−hd_2 not yet fitted (they will be fitted together with the two parameters k_1−k_2 belonging to *Hcp*, see step IV) while c_1−c_5 and d_1−d_4 are kept fixed, as their values are established in point II.

IV After incorporating the off-diagonal *Hcp* term, the model Hamiltonian is diagonalized to obtain simulated S_0 and S_1 adiabatic energies whose values depend on the six parameters (hc_1−hc_2, hd_1−hd_2, k_1−k_2) of $Hdir_{corr}$, Hct_{corr}, and *Hcp*. These parameter values are obtained by fitting the full data set plus additional 144 data set points obtained via 24 scans along the φ coordinate whose details are given in section S1 of the Supporting Information.

The fitting is performed using two utilities of the software *Mathematica*: *FindFit* and *NonlinearModelFit*. In both cases, the function minimizes a least-squares fit between the S_0 and S_1 adiabatic energies of the data set and the adiabatic energies from the model Hamiltonian. Since the converged parameter values may depend on the input values, we have achieved a steady and consistent result by trying several initial energy values (see section S2 in the Supporting Information). The final fitted parameters for PSB3 are given in Table1.

3. RESULTS AND DISCUSSION

In the present section, we start by looking at the accuracy (subsection 3.1) of the model Hamiltonian obtained after the fitting described in section 2. Next, in subsections 3.2 and 3.3, we discuss the topography of *Hdir*, *Hct*, and *Hcp* and the topography of the resulting simulated PSB3 force field. To do so, we look at the variations of the two-dimensional PES cross-section along r and θ as a function of φ.

3.1. Model accuracy. Below, we use the term "simulated" to indicate the data set values recomputed using the proposed model Hamiltonian with the parameters of Table 1. Figure 3A shows the S_0 (blue) and S_1 (red) energy profiles along the MEPcis (left), MEPtrans (right), and IS (center) paths. The figure shows that the parametrized H_{PSB3} function is capable to simulate the three sets of data with good accuracy. The same positive results is documented in Figure 3B and 3C for the MEPct and MEPdir profiles, respectively. Finally, the energy profile along BLAP is displayed in Figure 3D. Again, H_{PSB3} satisfactorily simulates the data set values.

Table 1. Optimum Parameters for H_{PSB3}

	PSB3
*hdir*2D	
d_1	2571
d_2	50.56
d_3	3.730
d_4	595.0
*hct*2D	
c_1	437.1
c_2	16.73
c_3	7.355
c_4	88.52
c_5	5.952
$hdir_{corr}$	
hd_1	37.58
hd_2	38.03
hct_{corr}	
hc_1	20.82
hc_2	21.21
hcp	
k_1	14.07
k_2	1.082

The H_{PSB3} accuracy has been evaluated quantitatively starting with *Hdir*2D and *Hct*2D. For these functions, the difference between data set and simulated values is ca. 1 kcal/mol (see section S3 in the Supporting Information). When $Hdir_{corr}$, Hct_{corr}, and *Hcp* are also considered, such difference increases, but the standard deviation remains lower than 2.5 kcal/mol, with only few values larger than 6 kcal/mol (see section S3 in the Supporting Information). We have found that the less accurate points belong to the φ scans, which are not part of the six data set paths. However, path regions, that are not well fitted, are found also in the last points of MEPdir and MEPct (see Figure 3C and 3D). The model fit these paths satisfactorily in the regions close the TSdir and TSct, that is the chemically relevant parts.

An independent test, providing information on the quality of the parametrization of H_{PSB3}, is the comparison between data set and simulated electronic characters. As explained above, the simulated values come from the H_{PSB3} eigenvectors that provide the weights of $\Psi_{COV/DIR}$ and Ψ_{CT} in each adiabatic state (Ψ_{S0} and Ψ_{S1}). The corresponding information can be extracted from the data set and compared with the simulated trend. For instance, when the charge on C2H−C1H−NH_2 is close to +1 or 0, we assign these points to pure $\Psi_{COV/DIR}$ or Ψ_{CT} states, respectively.

In Figure 4, we compare the data set (circles) and simulated (square) charge of the C2H−C1H−NH_2 moiety (i.e., the weight of the Ψ_{DIR} diabatic state). Although the parametrization is only based on adiabatic energies (i.e., no information is provided on the electronic character), the figure displays a qualitative agreement between data set and simulation, with the only exception of the initial parts of MEPcis and MEPtrans (see panel A in Figure 4). This disagreement is related to a model constrain (see point IV in subsection 2.2 discussing the parametrization constraints). In fact, as reported above, the initial 11 points along both paths were assumed to correspond to pure diabatic states. This

DOI: 10.1021/acs.jpca.8b10010
J. Phys. Chem. A 2019, 123, 1710−1719

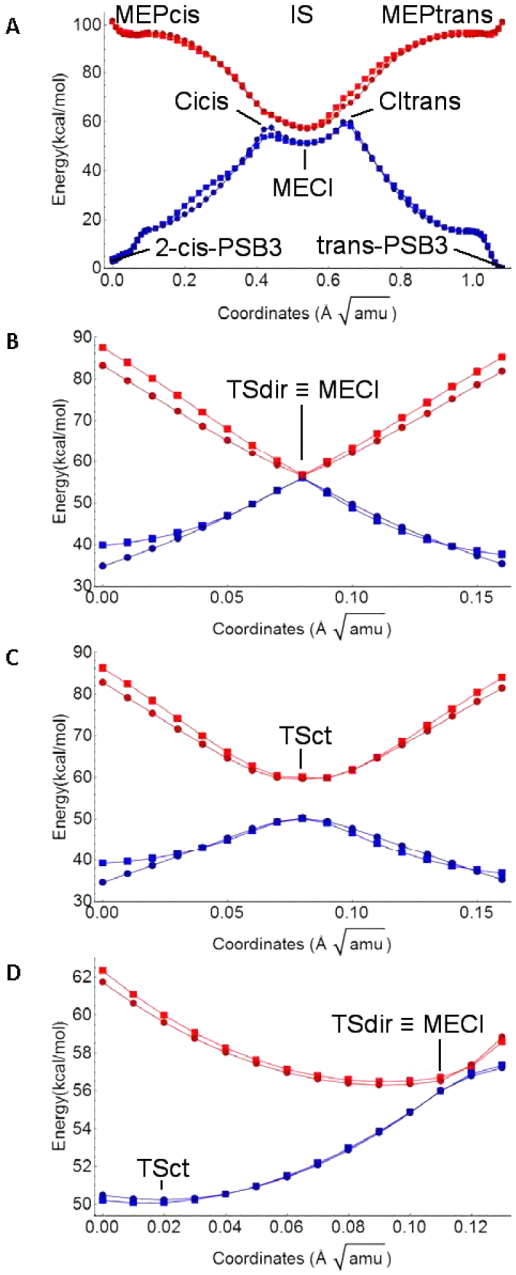

Figure 3. Comparison of data set (circles) and simulated (squares) adiabatic energy profiles along the six paths considered in this work. S_0 and S_1 profiles are in blue and red, respectively. (A) MEPcis, MEPtrans, and connecting IS profiles. The points include the 2-*cis*-PSB3 and all-*trans*-PSB3 equilibrium structures and the CIcis, CItrans, and MECI conical intersections. (B) MEPdir including the transition state TSdir. (C) MEPct including the transition state TSct. (D) BLAP energy including TSdir, TSct, and MECI.

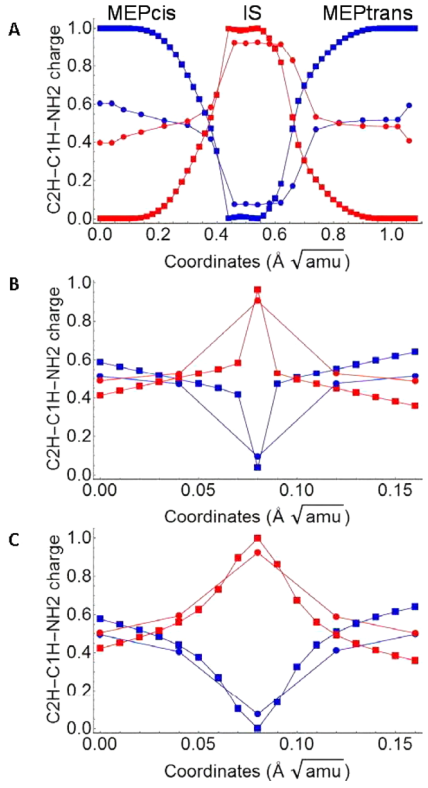

Figure 4. Comparison of data set (circles) and simulated (squares) $\Psi_{COV/DIR}$ weights (electronic characters). (A) MEPcis, MEPtrans and connecting IS. (B) MEPdir. (C) MEPct. Notice (see also text) that not all simulated points (squares) compare well with the data set points (circles).

assumption forces the simulated electronic character to be very different from the one displayed in the data set where the charge on the reference fragment is +0.6 (instead of +1) in S_0 and +0.4 (instead of 0) in S_1 in both 2-*cis* and all-*trans*-PSB3. However, the discrepancy between data set and simulated values decreases rapidly as one proceed along the two paths.

3.2. Parameter Sensitivity and Topography of the Diabatic PESs. Certain *Hdir*2D and *Hct*2D parameters are associated with specific features of the corresponding two-dimensional PESs. For instance, the value 0.091 in eq 4 defines the S_0 equilibrium r values of 2-*cis*-PSB3 and all-*trans*-PSB3 (this is treated as a constant specific to the system under investigation and it is, thus, not fitted), while d_3 determines the energy difference between the same two energy minima. In contrast, c_4 controls the vertical excitation energies of the same reactant and product minima. d_4 is the force constant of r mode of the two points of minima in the ground state, while c_1 is the same force constant evaluated at the two Franck–Condon (FC) points.

The S_1 and S_0 energy profiles along BLAP determine the sloped or peaked MECI topography that, in turn, reflects the relative stability of $\Psi_{COV/DIR}$ or Ψ_{CT} along the path. Such topography is controlled by d_2. More specifically, the Ψ_{DIR} energies are shifted at lower or higher values if d_2 increase or decrease, respectively. In this way, it is possible to define the energy of the BLAP minimum corresponding, in two- or three-dimensions, to TSdir. In a similar way c_3 determines the position of TSct.

In the Hct_{corr} and $Hdir_{corr}$ functions, φ changes the energy in a periodic fashion (see eqs 6 and 7). When $\theta = 0°$, $\pm 90°$ and $-180°$, a φ change produces a quadratic-like energy profile, with a vertex at $\varphi = 0°$ in both Hct_{corr} and $Hdir_{corr}$. As soon as the value of θ, starting from a value of 0°, approaches that of CIcis, such vertex moves to negative or positive φ values in $Hdir_{corr}$ and Hct_{corr}, respectively. In case we start from a value of $\theta = -180°$ and then approaching the θ value of CItras, such vertex moves to positive or negative φ values in $Hdir_{corr}$ and Hct_{corr}, respectively. These changes increase in magnitude until CIcis and CItrans are reached. Then, along IS, φ goes back

DOI: 10.1021/acs.jpca.8b10010
J. Phys. Chem. A 2019, 123, 1710–1719

toward a 0° value while θ proceeds toward a −90° value (i.e., toward the values of these variables at MECI).

The hd_1 and hc_1 parameters determine the concavity of the quadratic-like energy profile discussed above and can be interpreted as the "force constant" of the "φ mode". In contrast, the parameters hd_2 and hc_2 describe the shifting of its vertex as a function of θ. When one increases such parameters, the magnitude of φ at the CIcis and CItrans vertex is increased.

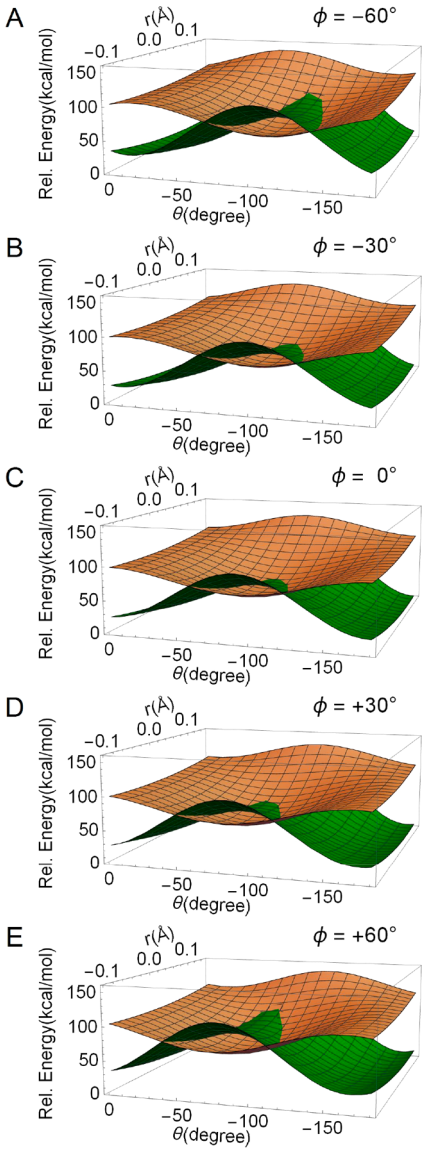

Figure 5. Two-dimensional cross sections of the diabatic PESs resulting from the parametrization of *Hct* and *Hdir* along r and θ. The different cross sections (i.e., from panel A to panel E) document the effect of φ on the PES topography and intersection. The Ψ_{CT} PES is displayed in brown, while the $\Psi_{COV/DIR}$ PES is displayed in green.

In Figure 5, we document the change in topography of the parametrized diabatic PESs (*Hdir* and *Hct*) along r, θ, and φ. Each panel shows their values as a function of r and θ. The different panels correspond to a different value of φ with the middle panel (i.e., panel C) corresponding to φ = 0°. The panels show how the seam between the two diabatic PESs moves. Indeed, the seam moves from $\theta > -90°$ when $\varphi > 0°$ to $\theta < -90°$ when $\varphi < 0°$. This feature is consistent with the IS data set that shows φ variations at each point. In fact, CIcis is characterized by a positive φ while CItrans by a negative value of φ. Thus, the seam characterized by different values of φ forms a surface (i.e., a two-dimensional set) of degenerate diabatic energies. As we discuss below, the coupling term *Hcp* transforms such surface into a curve (i.e., a one-dimensional set) of degenerate S_1 and S_0 adiabatic energies (i.e., of conical intersections) containing the IS path of the data set.

3.3. Parameters and Topography of the Off-Diagonal Matrix Element. The data set indicates that *Hcp* must vanish when the π-orbital overlap across the reacting C2 = C3 double bond is either zero (i.e., when the C2H−C1H−NH_2 and H_2C5−C4H−C3H π-orbitals are orthogonal) or maximized (i.e., the same π-orbitals are parallel). The first condition is satisfied at points such as MECI, TSct, and TSdir and at all points along the IS path. In contrast, the second condition is assumed to be true at the reactant and product S_0 equilibrium geometries (i.e., 2-*cis*-PSB3 and all-*trans*-PSB3 respectively) as in any other geometry which display maximum π-bonding (i.e., where φ = 0° and θ = 0° or θ = 180°). In all other structures $Hcp \neq 0$, the two diabatic states mix and the diabatic and adiabatic PESs become different.

Consistently with the above listed constraints, *Hcp* is written as a periodic function modulated by k_1, multiplied by a second scaling term that reaches a maximum value when $\theta = \pm 90°$ and that contains the k_2 parameter. As illustrated in Figure 6, as one moves off the MECI (i.e., off $\theta = -90°$ and $\varphi = 0$), the coupling becomes large in module. k_1 represents the amplitude of the sinusoidal function controlling such splitting (see eq 8). The sinusoid is maximized when $\theta - \varphi/2 = -45° \pm k\,\pi/2$, that is around the middle of the reaction paths. Finally, k_2 controls the effect of a periodic scaling that makes *Hcp* larger near $\theta = \pm 90°$. A better result can be obtained adding additional terms, for instance a sinusoid with maximum at $\theta - \varphi/2 = -45° \pm k\pi/4$. k_1 is an important parameter for the final accuracy of the model (see p-value in Table S2 of the Supporting Information); however, in order to simplify the reshaping to other force fields, it can be removed.

Each panel in Figure 6 is associated with a different value of φ and displays the *Hcp* as a function of r and θ. Inspection of the panels from top to bottom shows a strong dependency on the φ value. In contrast, and consistently with our assumption, the coupling is independent from r. Notice that, consistently with the IS path data set, the points where the coupling vanish (i.e., $Hcp = 0$) are shifted along θ when changing φ. For instance, CIcis has a $\theta \sim -70°$ and $\varphi \sim 36°$. The diagonalization of H_{PSB3} yields the adiabatic states expressed in terms of the square of *Hcp* and its sign has, thus, no significance.

3.4. Topography of the Simulated S_1 and S_0 Adiabatic PESs. The simulated adiabatic PESs obtained by solving the secular equation associated with H_{PSB3} are shown in Figure 7. As for Figure 5 and 6, each panel displays two-dimensional PES cross sections corresponding to different φ values. The secular equation also provides the simulated S_1 and S_0 adiabatic states (eigenvectors) expressed in terms of linear combinations of the $\Psi_{COV/DIR}$ and Ψ_{CT} diabatic states. The weights of $\Psi_{COV/DIR}$ and Ψ_{CT} are qualitatively represented with a color scale that highlights the percentage of covalent/diradical (green) and charge-transfer (brown) characters. Notice that, as stressed above and in order to decrease the mathematical complexity, we have imposed that the S_0 and S_1

DOI: 10.1021/acs.jpca.8b10010
J. Phys. Chem. A 2019, 123, 1710−1719

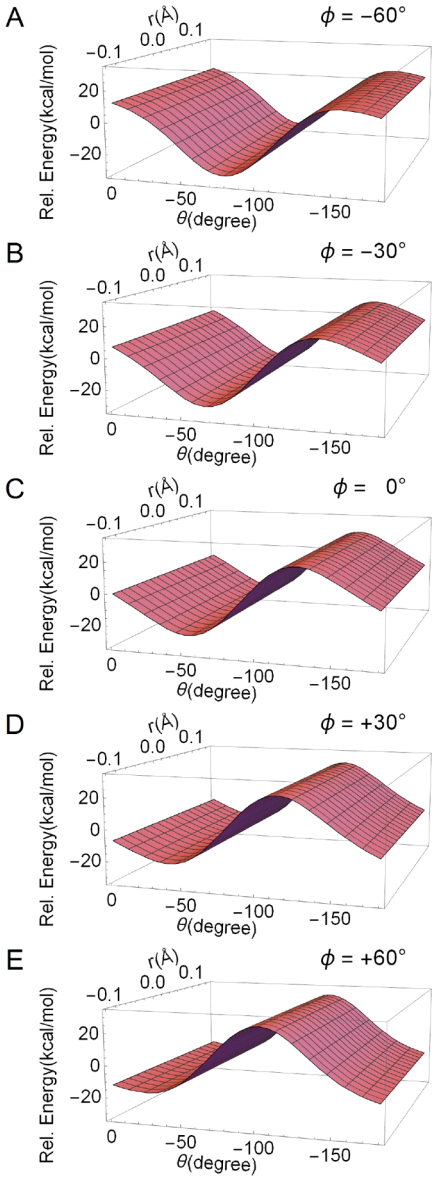

Figure 6. Two-dimensional cross-section of the coupling term *Hcp* as a function of *r* and *θ*. The different cross sections (i.e., from panel A to panel E) document the effect of *φ* on the *Hcp* surface topography. Notice that *Hcp* is independent from the *r* coordinate.

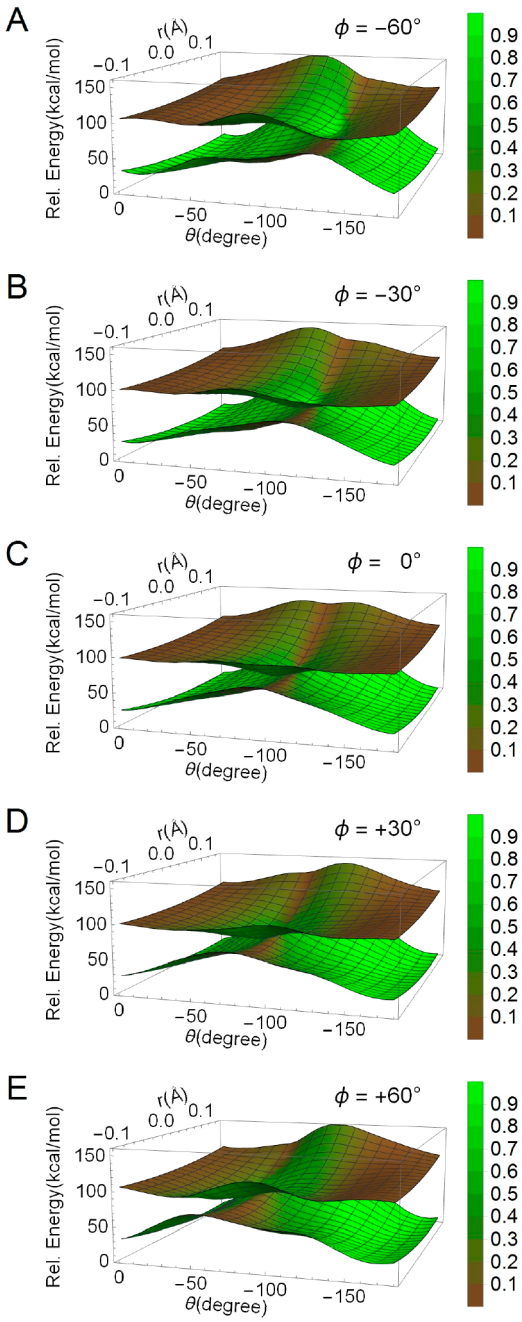

Figure 7. Two-dimensional cross sections of the simulated adiabatic PESs resulting from the parametrization of *Hct*, *Hdir* and *Hcp* along *r* and *θ*. The different cross sections (i.e., from panel A to panel E) document the effect of *φ* on the PES topography and conical intersection. The weight of the Ψ_{CT} character is displayed in brown, while the weight of the $\Psi_{COV/DIR}$ character is displayed in green. The legend on the right shows the eigenvector coefficients regarding the charge displaced in the C2H−C1H−NH2 moiety proportional to the $\Psi_{COV/DIR}$ weight.

states are characterized by pure $\Psi_{COV/DIR}$ and Ψ_{CT} states at the reactant and product structures, respectively.

The simulated electronic character is qualitatively consistent with those obtained from the data set (see also Figure 4). In other words, it is consistent with our understanding of the changes in electronic character along the S_1 isomerization paths and in the vicinity of conical intersection points. This can be seen in Figure 7, where on the S_1 PES one goes from a region dominated by Ψ_{CT} (i.e., in correspondence of the reactant and product geometries) to mixed $\Psi_{COV/DIR}$ and Ψ_{CT} regions when moving toward the transition states. Furthermore, it is evident that along any S_1 walk forming a loop encircling a conical intersection point, the S_1 or S_0 character moves from regions with charge-transfer character to regions with a pure covalent/diradical character and again to regions with charge transfer character or vice versa. This behavior is consistent with the theory of conical intersections (e.g., the existence of a geometric phase) and must occur in opposite directions in S_1 and S_0.

4. CONCLUSIONS

We have provided a mathematical expression for the first two adiabatic PESs of PSB3: a minimal model of the chromophore of the retina visual pigment of vertebrate and invertebrates. The employed Hamiltonian, which is based on a diabatic

DOI: 10.1021/acs.jpca.8b10010
J. Phys. Chem. A 2019, 123, 1710−1719

representation where each diabatic state corresponds to a specific electronic character (i.e., either covalent/diradical or charge-transfer), is a function of three different geometrical modes. After the parametrization, the simulated S_0 and S_1 adiabatic energies show a good correlation with the corresponding data set points computed at the XMCQDPT2/6-31G* level of theory. This is especially true in regions close to reaction paths (with differences close to 2 kcal/mol), while less precise results are found far from the paths and along φ deformations.

Relative to the model of Stock, we have improved the model physics by (i) fitting accurate data set points, (ii) including an extra degree of freedom which is known to play a fundamental role in the isomerization processes, and (iii) incorporating information on the change in electronic distribution along the adiabatic PESs. Future developments of the model could include the increase in the number of states to achieve a three-state three-mode model, which appears to be necessary for studying rhodopsins different from visual pigments. Moreover, we wish to make the model adjustable. In other words, we wish to introduce parameters that can introduce predictable variations in the topology and topography of the adiabatic PESs. In this way researchers may use the model as a basis for simulating the PESs of chromophore models with a conjugated π-system longer than PSB3, the effect of certain substituents or the effect of the presence of a complex environment. It may also be possible to generate models for different biological chromophores.[36] Finally, and most importantly, the model developed here, or any suitably adjusted model derived from it, could be used to perform quantum dynamics calculation with traditional or novel methods requiring analytical PESs.[22,37]

Finally, we have to warn the reader that, according to recent reports[38,39] and in contrast with the rhodopsins of superior animals where only two electronic states (the S_0 and S_1 states) are mainly driving the isomerization process, the photoinduced microbial rhodopsin dynamics often display the involvement of a third state (S_2). Thus, PSB3, which has an S_2 state higher[11,40] and not interacting with the S_1 state along the six reaction paths parametrized above (see the extensive 3-root state-average XMCQDPT2 mapping in section S4 of the Supporting Information) provides a model of rhodopsins where S_1 never interact with S_2. A future parametrization project in our lab will address the issue of generalizing the presented two-state three-mode model to a three-state three-mode model also applicable to microbial rhodopsins.

■ ASSOCIATED CONTENT

Supporting Information

The Supporting Information is available free of charge on the ACS Publications Web site. The Supporting Information is available free of charge on the ACS Publications website at DOI: 10.1021/acs.jpca.8b10010.

Details of (i) the rigid φ scan, (ii) the starting values for the fitting procedures, and (iii) the deviation between model and data set (PDF)

■ AUTHOR INFORMATION

Corresponding Author

*(M.O.) E-mail: molivuc@bgsu.edu; massimo.olivucci@unisi.it.

ORCID

Marwa H. Farag: 0000-0003-0443-1089

Luca De Vico: 0000-0002-2821-5711

Massimo Olivucci: 0000-0002-8247-209X

Author Contributions

E.M. and M.H.F. equally contributed to the present work.

Notes

The authors declare no competing financial interest.

■ ACKNOWLEDGMENTS

The authors are indebted to Dr. Samer Gozem of Georgia State University for a critical reading of the manuscript. E.M., L.D.V. and M.O. acknowledge MIUR (Ministero dell'Istruzione, dell'Università e della Ricerca) Grant "Dipartimento di Eccellenza 2018−2022". The research has been partially supported by the following grants MIUR (PRIN 2015) NSF CHE-CLP-1710191, and NIH 1R15GM126627 01. M.O. is also grateful for an USIAS 2015 fellowship.

■ REFERENCES

(1) Vreven, T.; Bernardi, F.; Garavelli, M.; Olivucci, M.; Robb, M. A.; Schlegel, H. B. Ab Initio Photoisomerization Dynamics of a Simple Retinal Chromophore Model. *J. Am. Chem. Soc.* **1997**, *119*, 12687−12688.

(2) Garavelli, M.; Bernardi, F.; Robb, M. A.; Olivucci, M. The short-chain acroleiniminium and pentadieniminium cations: towards a model for retinal photoisomerization. A CASSCF/PT2 study. *J. Mol. Struct.: THEOCHEM* **1999**, *463*, 59−64.

(3) Page, C. S.; Olivucci, M. Ground and excited state CASPT2 geometry optimizations of small organic molecules. *J. Comput. Chem.* **2003**, *24*, 298−309.

(4) Sinicropi, A.; Migani, A.; De Vico, L.; Olivucci, M. Photoisomerization Acceleration in Retinal Protonated Schiff-base Models. *Photochem. Photobiol. Sci.* **2003**, *2*, 1250−1255.

(5) Fantacci, S.; Migani, A.; Olivucci, M. CASPT2//CASSCF and TDDFT//CASSCF Mapping of the Excited State Isomerization Path of a Minimal Model of the Retinal Chromophore. *J. Phys. Chem. A* **2004**, *108*, 1208−1213.

(6) Barbatti, M.; Ruckenbauer, M.; Szymczak, J. J.; Aquino, A. J. A.; Lischka, H. Nonadiabatic excited-state dynamics of polar pi-systems and related model compounds of biological relevance. *Phys. Chem. Chem. Phys.* **2008**, *10*, 482−494.

(7) Mori, T.; Nakano, K.; Kato, S. Conical intersections of free energy surfaces in solution: effect of electron correlation on a protonated Schiff base in methanol solution. *J. Chem. Phys.* **2010**, *133*, 064107.

(8) Valsson, O.; Filippi, C. Photoisomerization of Model Retinal Chromophores: Insight from Quantum Monte Carlo and Multi-configurational Perturbation Theory. *J. Chem. Theory Comput.* **2010**, *6*, 1275−1292.

(9) De Vico, L.; Page, C. S.; Garavelli, M.; Bernardi, F.; Basosi, R.; Olivucci, M. Reaction Path Analysis of the "Tunable" Photoisomerization Selectivity of Free and Locked Retinal Chromophores. *J. Am. Chem. Soc.* **2002**, *124*, 4124−4134.

(10) De Vico, L.; Garavelli, M.; Bernardi, F.; Olivucci, M. Photoisomerization mechanism of 11-cis-locked artificial retinal chromophores: acceleration and primary photoproduct assignment. *J. Am. Chem. Soc.* **2005**, *127*, 2433−2442.

(11) Gozem, S.; Huntress, M.; Schapiro, I.; Lindh, R.; Granovsky, A.; Angeli, C.; Olivucci, M. Dynamic Electron Correlation Effects on the Ground State Potential Energy Surface of a Retinal Chromophore Model. *J. Chem. Theory Comput.* **2012**, *8*, 4069−4080.

(12) Gozem, S.; Melaccio, F.; Lindh, R.; Krylov, A. I.; Granovsky, A. A.; Angeli, C.; Olivucci, M. Mapping the excited state potential energy surface of a retinal chromophore model with multireference and equation-of-motion coupled-cluster methods. *J. Chem. Theory Comput.* **2013**, *9*, 4495−4506.

DOI: 10.1021/acs.jpca.8b10010
J. Phys. Chem. A 2019, 123, 1710−1719

(13) Huix-Rotllant, M.; Filatov, M.; Gozem, S.; Schapiro, I.; Olivucci, M.; Ferré, N. Assessment of Density Functional Theory for Describing the Correlation Effects on the Ground and Excited State Potential Energy Surfaces of a Retinal Chromophore Model. *J. Chem. Theory Comput.* **2013**, *9*, 3917−3932.
(14) Gozem, S.; Melaccio, F.; Valentini, A.; Filatov, M.; Huix-Rotllant, M.; Ferré, N.; Frutos, L. M.; Angeli, C.; Krylov, A. I.; Granovsky, A. A.; Lindh, R.; Olivucci, M. Shape of Multireference, EOM-CC, and DFT Potential Energy Surfaces at a Conical Intersection. *J. Chem. Theory Comput.* **2014**, *10*, 3074−3084.
(15) Tuna, D.; Lefrancois, D.; Wolanski, L.; Gozem, S.; Schapiro, I.; Andruniów, T.; Dreuw, A.; Olivucci, M. Assessment of Approximate Coupled-Cluster and Algebraic-Diagrammatic-Construction Methods for Ground-and Excited-State Reaction Paths and the Conical-Intersection Seam of a Retinal-Chromophore Model. *J. Chem. Theory Comput.* **2015**, *11*, 5758−5781.
(16) Zen, A.; Coccia, E.; Gozem, S.; Olivucci, M.; Guidoni, L. Quantum Monte Carlo Treatment of the Charge Transfer and Diradical Electronic Character in a Retinal Chromophore Minimal Model. *J. Chem. Theory Comput.* **2015**, *11*, 992−1005.
(17) Werner, H.; Knowles, P. J. An efficient internally contracted multiconfiguration−reference configuration interaction method. *J. Chem. Phys.* **1988**, *89*, 5803−5814.
(18) Werner, H.-J.; Kállay, M.; Gauss, J. The barrier height of the F +H2 reaction revisited: Coupled-cluster and multireference configuration-interaction benchmark calculations. *J. Chem. Phys.* **2008**, *128*, 034305.
(19) Atchity, G. J.; Xantheas, S. S.; Ruedenberg, K. Potential energy surfaces near intersections. *J. Chem. Phys.* **1991**, *95*, 1862−1876.
(20) Hahn, S.; Stock, G. Quantum-mechanical modeling of the femtosecond isomerization in rhodopsin. *J. Phys. Chem. B* **2000**, *104*, 1146−1149.
(21) Tscherbul, T. V.; Brumer, P. Excitation of Biomolecules with Incoherent Light: Quantum Yield for the Photoisomerization of Model Retinal. *J. Phys. Chem. A* **2014**, *118*, 3100−3111.
(22) Curchod, B. F. E.; Agostini, F. On the Dynamics through a Conical Intersection. *J. Phys. Chem. Lett.* **2017**, *8*, 831−837.
(23) Johnson, P. J. M.; Farag, M. H.; Halpin, A.; Morizumi, T.; Prokhorenko, V. I.; Knoester, J.; Jansen, T. L. C.; Ernst, O. P.; Miller, R. J. D. The primary photochemistry of vision occurs at the molecular speed limit. *J. Phys. Chem. B* **2017**, *121*, 4040−4047.
(24) Abe, M.; Ohtsuki, Y.; Fujimura, Y.; Domcke, W. Optimal control of ultrafast cis-trans photoisomerization of retinal in rhodopsin via a conical intersection. *J. Chem. Phys.* **2005**, *123*, 144508.
(25) Farag, M. H.; Jansen, T. L. C.; Knoester, J. Probing the Interstate Coupling near a Conical Intersection by Optical Spectroscopy. *J. Phys. Chem. Lett.* **2016**, *7*, 3328−3334.
(26) Farag, M. H.; Jansen, T. L. C.; Knoester, J. The origin of absorptive features in the two-dimensional electronic spectra of rhodopsin. *Phys. Chem. Chem. Phys.* **2018**, *20*, 12746−12754.
(27) Seidner, L.; Domcke, W. Microscopic modelling of photoisomerization and internal-conversion dynamics. *Chem. Phys.* **1994**, *186*, 27−40.
(28) Granovsky, A. A. Extended multi-configuration quasi-degenerate perturbation theory: The new approach to multi-state multi-reference perturbation theory. *J. Chem. Phys.* **2011**, *134*, 214113−214127.
(29) Shiozaki, T.; Werner, H.-J. Explicitly correlated multireference configuration interaction with multiple reference functions: Avoided crossings and conical intersections. *J. Chem. Phys.* **2011**, *134*, 184104.
(30) Granovsky, A. A. *Firefly*, version 8.2.0 http://classic.chem.msu.su/gran/firefly/index.html (accessed 1st September 2017), 2012.
(31) Schmidt, M. W.; Baldridge, K. K.; Boatz, J. A.; Elbert, S. T.; Gordon, M. S.; Jensen, J. H.; Koseki, S.; Matsunaga, N.; Nguyen, K. A.; Su, S.; et al. General atomic and molecular electronic structure system. *J. Comput. Chem.* **1993**, *14*, 1347−1363.
(32) Vlaisavljevich, B.; Shiozaki, T. Nuclear Energy Gradients for Internally Contracted Complete Active Space Second-Order Perturbation Theory: Multistate Extensions. *J. Chem. Theory Comput.* **2016**, *12*, 3781−3787.
(33) Michl, J.; Bonačić-Koutecký, V. *Electronic aspects of organic photochemistry*; Wiley: New York, 1990.
(34) Köppel, H. Diabatic Representation: Methods for the Construction of Diabatic Electronic State. *Conical Intersections: Electronic Structure, Dynamics and Spectroscopy* **2004**, *15*, 175−204.
(35) Woywod, C.; Domcke, W.; Sobolewski, A. L.; Werner, H. Characterization of the S1−S2 conical intersection in pyrazine using ab initio multiconfiguration self-consistent-field and multireference configuration-interaction methods. *J. Chem. Phys.* **1994**, *100*, 1400−1413.
(36) Gozem, S.; Luk, H. L.; Schapiro, I.; Olivucci, M. Theory and Simulation of the Ultrafast Double-Bond Isomerization of Biological Chromophores. *Chem. Rev.* **2017**, *117*, 13502−13565.
(37) Sala, M.; Egorova, D. Quantum dynamics of multi-dimensional rhodopsin photoisomerization models: Approximate versus accurate treatment of the secondary modes. *Chem. Phys.* **2018**, *515*, 164−176.
(38) Luk, H. L.; Melaccio, F.; Rinaldi, S.; Gozem, S.; Olivucci, M. Molecular bases for the selection of the chromophore of animal rhodopsins. *Proc. Natl. Acad. Sci. U. S. A.* **2015**, *112*, 15297−15302.
(39) Marín, M. d. C.; Agathangelou, D.; Orozco-Gonzalez, Y.; Valentini, A.; Kato, Y.; Abe-Yoshizumi, R.; Kandori, H.; Choi, A.; Jung, K.-H.; Haacke, S.; Olivucci, M. Fluorescence Enhancement of a Microbial Rhodopsin via Electronic Reprogramming. *J. Am. Chem. Soc.* **2019**, *141*, 262−271.
(40) Garavelli, M.; Celani, P.; Bernardi, F.; Robb, M. A.; Olivucci, M. The C5H6NH2+ Protonated Shiff Base: An ab Initio Minimal Model for Retinal Photoisomerization. *J. Am. Chem. Soc.* **1997**, *119*, 6891−6901.

DOI: 10.1021/acs.jpca.8b10010
J. Phys. Chem. A 2019, 123, 1710−1719